CHEMISTRY

Direct growth of wafer-scale highly oriented graphene on sapphire

Zhaolong Chen[1,2,3], Chunyu Xie[1,4], Wendong Wang[5], Jinpei Zhao[6], Bingyao Liu[4,7], Jingyuan Shan[1,2], Xueyan Wang[8], Min Hong[1,4], Li Lin[3], Li Huang[8], Xiao Lin[8], Shenyuan Yang[9,10]*, Xuan Gao[2], Yanfeng Zhang[1,2,4]*, Peng Gao[2,7,11,12]*, Kostya S. Novoselov[3,13]*, Jingyu Sun[2,14]*, Zhongfan Liu[1,2]*

Direct chemical vapor deposition (CVD) growth of wafer-scale high-quality graphene on dielectrics is of paramount importance for versatile applications. Nevertheless, the synthesized graphene is typically a polycrystalline film with high density of uncontrolled defects, resulting in a low carrier mobility and high sheet resistance. Here, we report the direct growth of highly oriented monolayer graphene films on sapphire wafers. Our growth strategy is achieved by designing an electromagnetic induction heating CVD operated at elevated temperature, where the high pyrolysis and migration barriers of carbon species are easily overcome. Meanwhile, the embryonic graphene domains are guided into good alignment by minimizing its configuration energy. The thus obtained graphene film accordingly manifests a markedly improved carrier mobility (~14,700 square centimeters per volt per second at 4 kelvin) and reduced sheet resistance (~587 ohms per square), which compare favorably with those from catalytic growth on polycrystalline metal foils and epitaxial growth on silicon carbide.

INTRODUCTION

Graphene has high carrier mobility, good mechanical robustness, and high optical transparency, holding promise for applications in high-frequency transistors (*1*, *2*) and transparent conductive electrodes (*3*). In addition, the linear dispersion of the Dirac electrons of graphene also enables target devices such as photodetectors (*4*) and optical modulators (*5*). For most of these applications, attaining wafer-scale single-crystal graphene without breakages and contaminations on dielectric substrates is a prerequisite (*1*, *6*, *7*). Wafer-sized, high-mobility graphene has readily been produced on SiC by sublimation of silicon atoms (*8*–*11*). Nevertheless, the layer number uniformity is still unsatisfactory over the entire wafer (*12*). Moreover, the high cost of SiC and its niche marketing in consumer electronics brings an insurmountable challenge for the mass production and commercialization (*13*). Meanwhile, chemical vapor deposition (CVD) technology involves cumbersome and destructive transfer processes from metal substrates (e.g., Cu, Ni, and their alloys) to dielectric ones, although the former typically enables higher quality of graphene (*14*–*17*). In this respect, the direct growth of graphene harnessing favorable quality over dielectric substrates has emerged as an ideal route to bypass transfer-related issues.

The direct synthesis of graphene on SiO_2 (*18*), hexagonal BN (h-BN) (*19*), TiO_2 (*20*, *21*), and glass (*22*) by conventional CVD techniques has been achieved. Nevertheless, because of the lacking of catalytic activity and universal potential field of substrates, the as-produced films are typically polycrystalline consisted of randomly orientated small domains with uncertain thickness that has a high density of grain boundaries, atomic vacancies, and impurities and, hence, an unsatisfactory crystal quality. Even by introducing a remote metal catalyst (*23*, *24*) and investigating feedstock sources (*25*, *26*), the carrier mobility [800 $cm^2 V^{-1} s^{-1}$ in (*23*) and 3800 $cm^2 V^{-1} s^{-1}$ in (*25*)] and sheet resistance [1100 ohms $\square^{-1}$ at 93% transparency in (*26*)] of as-grown graphene have not improved substantially. In the realm of single crystal growth, epitaxy is an affordable method for the growth of high quality semiconductor films with well-defined orientations. *c*-plane (0001) sapphire is a low-cost single-crystal dielectric substrate, holding a broad application prospect in integrated circuits (*27*) and optoelectronic devices (*28*). However, previous attempts to grow graphene on sapphire (0001) have failed to achieve well-aligned nucleation and large domain size, accompanied by the formation of abundant unwanted grain boundaries (*13*, *29*, *30*). In addition, the relatively lower reaction temperature of normal CVD system leads to the slow growth rate due to the high decomposition energy and large diffusion barriers of carbon precursors on sapphire (*31*, *32*). Therefore, how to fast grow the aligned nucleated domains, increase the individual domain size, and form a continuous uniform monolayer film at a wafer scale is a main hurdle to overcome.

In this contribution, we present the direct growth of wafer-scale continuous, highly oriented, monolayer graphene films with large domain size on *c*-plane sapphire via an electromagnetic induction heating CVD method, which can extend the growth parameter space (i.e., higher temperatures) as compared to normal reactors.

[1]Center for Nanochemistry (CNC), Beijing Science and Engineering Center for Nanocarbons, Beijing National Laboratory for Molecular Sciences, College of Chemistry and Molecular Engineering, Peking University, Beijing 100871, China. [2]Beijing Graphene Institute (BGI), Beijing 100095, China. [3]Institute for Functional Intelligent Materials, National University of Singapore, Singapore 117575, Singapore. [4]Academy for Advanced Interdisciplinary Studies, Peking University, Beijing 100871, China. [5]School of Physics and Astronomy, University of Manchester, Manchester M13 9PL, UK. [6]Department of Physics, National University of Singapore, Singapore 117551, Singapore. [7]Electron Microscopy Laboratory and International Center for Quantum Materials, School of Physics, Peking University, Beijing 100871, China. [8]Institute of Physics, Chinese Academy of Sciences, Beijing 100190, China. [9]State Key Laboratory of Superlattices and Microstructures, Institute of Semiconductors, Chinese Academy of Sciences, Beijing 100083, China. [10]Center of Materials Science and Optoelectronics Engineering, University of Chinese Academy of Sciences, Beijing 100049, China. [11]Collaborative Innovation Center of Quantum Matter, Beijing 100871, China. [12]Interdisciplinary Institute of Light-Element Quantum Materials and Research Center for Light-Element Advanced Materials, Peking University, Beijing 100871,China. [13]Chongqing 2D Materials Institute, Liangjiang New Area, Chongqing 400714, China. [14]College of Energy, Soochow Institute for Energy and Materials Innovations (SIEMIS), Key Laboratory of Advanced Carbon Materials and Wearable Energy Technologies of Jiangsu Province, Soochow University, Suzhou 215006, China.
*Corresponding author. Email: syyang@semi.ac.cn (S.Y.); yanfengzhang@pku.edu.cn (Y.Z.); p-gao@pku.edu.cn (P.G.); kostya@nus.edu.sg (K.S.N.); sunjy86@suda.edu.cn (J.S.); zfliu@pku.edu.cn (Z.L.)

With an optimized growth process, the kinetics and thermodynamics are conducive to high-quality graphene growth: The high reaction energy barriers of methane (CH_4) pyrolysis and active carbon species migration are overcome by an elevated growth temperature, allowing sufficient generation and fast diffusion of active carbon on the surface of substrate; the graphene-Al_2O_3 (0001) interface reaches its minimum energy configuration when graphene domains crystallographically align with sapphire; and the gas-phase side reactions leading to the formation of amorphous carbon and multilayer nucleation are suppressed by reduced gas-phase temperature in our cold wall design. Consequently, wafer-scale high-quality monolayer graphene is obtained within a short growth duration of 30 min, showing a high carrier mobility (~14,700 $cm^2\ V^{-1}\ s^{-1}$) and a low sheet resistance (~587 ohms $\square^{-1}$). This reliable approach of direct growth of highly oriented graphene films on sapphire wafers paves the route toward emerging graphene electronics and photonics.

RESULTS

In our solution to wafer-scale high-quality graphene growth, we use electromagnetic induction heating as the heater source of the cold wall CVD system to extend the growth parameter space in comparison with the hot wall reactors (Fig. 1A and fig. S1). Our homemade CVD reactor enables a quick temperature ramping to 1400°C within 10 min (maximum heating rate, ~200°C min^{-1}). Note that this growth temperature is markedly higher than that of the hot wall counterparts and is the key to obtaining highly orientated graphene domains, as demonstrated vide infra. Moreover, our cold wall reactor also enables the confinement of thermal energy at the sapphire substrate. This would substantially reduce the temperature of the gas phase (Fig. 1, B and C), suppressing the adverse gas-phase side reactions that always incur the formation of multilayer nucleation and amorphous carbon (*33*). In this sense, our process offers precise control over active carbon supply, and hence, homogeneous growth of monolayer graphene is achievable.

Then, to provide guidance regarding the role of sapphire in graphene formation, we carried out first-principles calculations based on density functional theory (DFT) to reveal the preferable orientation of the graphene domain on sapphire. We modeled the adsorption of a small graphene cluster ($C_{24}H_{12}$) on an Al_2O_3 (0001) slab, where the surface was constructed by a (3 × 3) supercell. Here, the most stable Al_2O_3 (0001) surface was terminated by one Al atom in each unit cell (named as the low Al atom), as revealed in previous reports (*34*, *35*), and the $C_{24}H_{12}$ cluster containing 24 carbon atoms was considered a typical nucleation seed for modeling, with the edge passivated by H atoms to avoid edge effects. Our calculations show that the $C_{24}H_{12}$ cluster prefers to adsorb on the Al_2O_3 surface with one C atom on top of the surface low Al atom (fig. S2). We thus considered two configurations, as shown in Fig. 1D: one with an edge C atom (C1) on top of the low Al atom and the other with a centered C atom (C2) on top of the low Al atom. We then fixed the in-plane coordinates of the C1 or C2 atom and rotated the cluster with different rotational angles θ from 0° to 60°. Here, θ is the angle between the in-plane lattice vectors of graphene and sapphire. The in-plane coordinates of another C atom were also kept fixed to maintain the rotational angle during relaxation. Because of this constraint, the relative energies were not symmetric with respect to θ = 30° (Fig. 1E). However, we can clearly see that θ = 30° is the most stable configuration, while θ = 0° and 60° corresponds to local minima. We further released the above constraint and fully relaxed

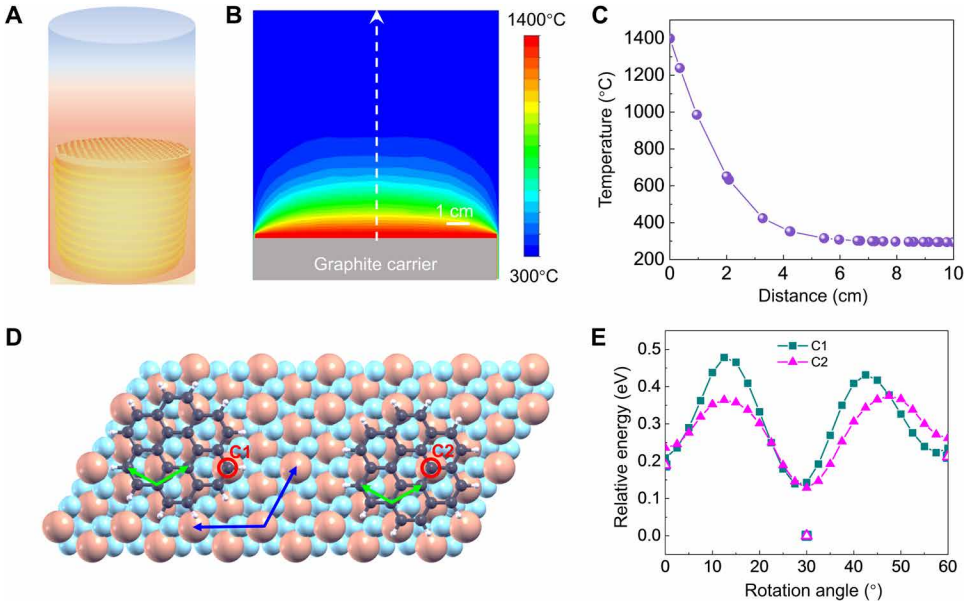

Fig. 1. Mechanism of alignment of graphene domains on Al_2O_3 (0001) substrate. (**A**) The schematic of the homemade induction heating CVD reactor, where sapphire substrate is directly placed on the graphite carrier that is surrounded with induction coil. (**B** and **C**) The simulated temperature distribution of the induction heating cold wall CVD system (at 1400°C, 2000 Pa) (B) and the corresponding temperature profile against the distance from graphite carrier (C). (**D**) Two configurations of graphene cluster $C_{24}H_{12}$ adsorbed on a sapphire (0001) substrate with a rotational angle of 30°. C1 and C2 denote the C atoms on top of the surface low Al atom. The lattice vectors of graphene and sapphire (0001) are labeled as green and blue arrows, respectively. (**E**) First-principles calculations of the relative energies of graphene cluster $C_{24}H_{12}$ on an Al_2O_3 (0001) substrate with various rotational angles. The hollow circles and squares correspond to the unconstrained configurations at 0°, 30°, and 60°.

the graphene cluster (fig. S3) and found that the configuration at θ = 30° is more stable than those at 0° and 60° by ca. 0.2 eV (hollow symbols in Fig. 1E). Therefore, we concluded that θ = 30° is the most stable orientation of graphene on a sapphire (0001) substrate. We also estimated the rotational barrier from the local minima (0° and 60°) to the global minimum (30°) to be about 0.1 to 0.2 eV (Fig. 1E). The reversed process had a higher barrier and does not occur as readily. It is reasonable to speculate that high temperature (here 1400°C) is helpful to reach the energetically preferable configuration for graphene nuclei, greatly contributing to the alignment of graphene domains at the embryonic stage. Therefore, the growth of wafer-sized highly oriented graphene on sapphire is achievable following an interface coupling–guided growth mechanism.

The elevated growth temperature gave rise to a sufficient pyrolysis of CH_4 and an efficient migration of adsorbed active carbon species on sapphire substrate, thereby promoting the growth rate and crystal quality. Temperature-dependent growth results are collected in fig. S4. Under optimized conditions, a continuous graphene film covers the 2-inch sapphire wafer within 30 min (fig. S5), displaying high transparency to the naked eye (Fig. 2A). The derived growth rate is nearly 10 times faster than that for growth on a dielectric substrate by the common hot wall CVD method (*32*, *36*). Scanning electron microscopy (SEM) over thousands of square micrometers shows a homogeneous contrast, suggesting that the monolayer graphene at a full coverage is formed without any voids (Fig. 2B and inset). Figure 2C shows the typical Raman spectra of the graphene directly produced on sapphire measured from representative positions (marked in Fig. 2A). It is evident that all the spectra display the identically featured Raman signals of graphene (G band at ~1582 cm^{-1} and 2D band at ~2670 cm^{-1}; the full width at half maximum of the 2D band is ~35 cm^{-1}), confirming the uniformity of the as-grown graphene over the wafer scale. The absence of the D peak and high intensity of the 2D peak imply that a high-quality monolayer of graphene was obtained, despite the fact that no metal catalyst was used during synthesis (fig. S6). Raman maps of I_{2D}/I_G and I_G over a 10 μm by 10 μm area further verify the high uniformity and favorable quality, where the value of I_{2D}/I_G is higher than 2 (Fig. 2D and fig. S7).

In contrast to epitaxial growth on SiC, on which the uncontrollable thermal decomposition of SiC underneath the epitaxial graphene layers (*37*) and step bunching process (*38*) would normally induce nonuniform film thickness, our CVD strategy offers precise control over the formation of monolayer graphene. The optical microscopy (OM) image shows a uniform optical contrast after being transferred onto SiO_2/Si substrates (Fig. 2E), where no contamination or second layers are visible. Both the atomic force microscopy (AFM) height profile (Fig. 2F) and visible light transmittance spectrum (fig. S8) manifest the characteristics of monolayer graphene. The wrinkles shown in the AFM image are due to the mismatch of thermal expansion coefficients between the graphene and substrate, which is a ubiquitous phenomenon for graphene grown by CVD method. Moreover, Fig. 2G presents a cross-sectional transmission electron microscopy (TEM) image of the graphene/sapphire interface, demonstrating high uniformity without discernible contamination. Note that, in a conventional hot wall reactor, the temperature of the gas phase above the growth substrate is relatively high to spur the generation of large-sized carbon clusters, initiating the formation of amorphous carbon and multilayer nucleation (fig. S9). Therefore,

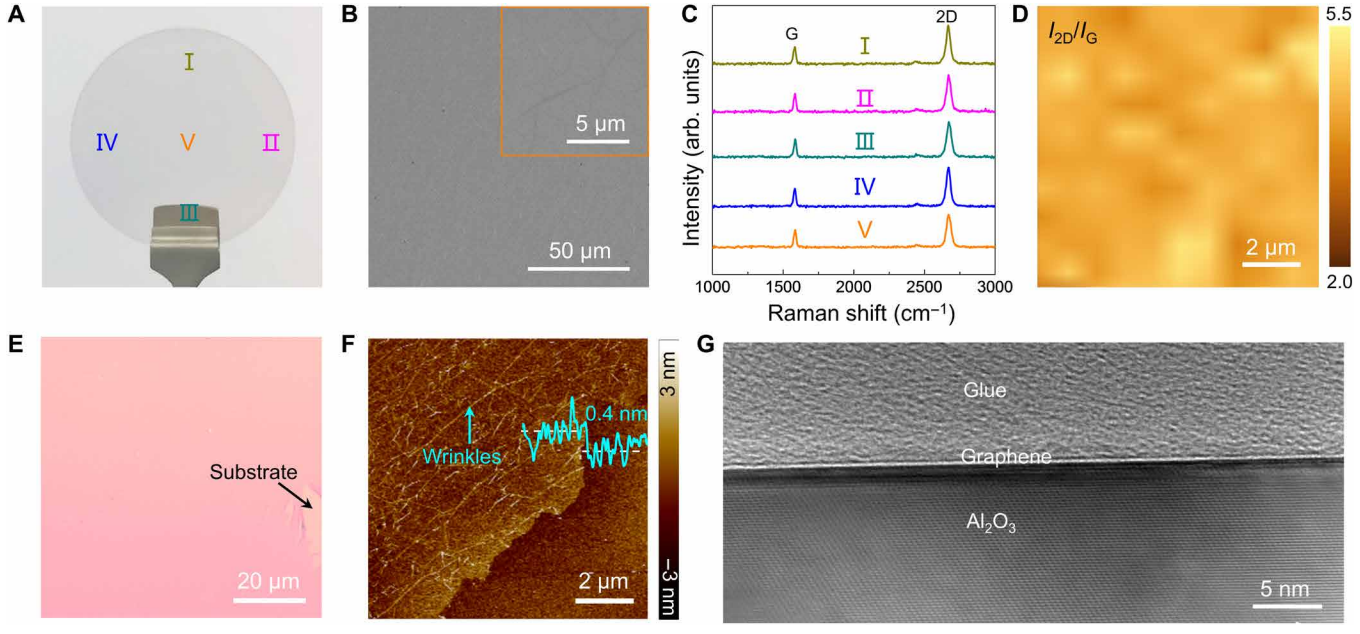

Fig. 2. Direct growth of a monolayer graphene film on sapphire wafer by electromagnetic induction heating CVD. (**A**) A typical photograph of an as-grown 2-inch graphene/sapphire wafer. Photo credit: Zhaolong Chen, Peking University. (**B**) Typical SEM image of as-grown graphene on sapphire. The inset shows the high-magnification SEM image of graphene. (**C**) Raman spectra of as-grown graphene measured from representative positions labeled in (A). arb. units, arbitrary units. (**D**) Raman I_{2D}/I_G map of as-grown graphene films on sapphire. (**E**) Optical microscopy (OM) image of the as-grown graphene after transfer onto a SiO_2/Si substrate. (**F**) Atomic force microscopy (AFM) height image of as-grown graphene after transfer onto a SiO_2/Si substrate. (**G**) High-resolution cross-sectional transmission electron microscopy (TEM) image of as-grown graphene on sapphire.

we can conclude that the growth of graphene on sapphire, in our case, obeys a typical surface-limited growth mode. Such a growth is enabled by the absence of large carbon clusters in gas phase and the presence of high adsorption energy barrier on graphene for carbon species, which allows the individual carbons reaching on the surface of graphene to quickly migrate to the edge of graphene.

To unravel the lattice orientations of the as-grown monolayer graphene on sapphire, we thus performed low-energy electron diffraction (LEED) characterizations with the spot size of approximately 1 mm in diameter. Because of the size limitation of the sample holder, as-grown wafer-size graphene was cut into 5 mm by 5 mm pieces. LEED patterns collected from all these pieces are coincident. One typical set of diffraction pattern shows six slightly dispersive spots arranged in a hexagonal rather than ring-shaped patterns, suggesting the predominant orientation of the graphene films. Furthermore, the diffraction patterns obtained from different areas demonstrated no noticeable changes (Fig. 3, A to D), revealing the highly oriented nature of the wafer-sized graphene. We found that the graphene unit cells were mainly rotated by 30° with respect to the sapphire; the armchair and zigzag directions of the graphene lattice were parallel to the [01$\bar{1}$0] and [21$\bar{3}$0] directions of the Al_2O_3 (0001), respectively, in good agreement with foregoing DFT calculation results. The lattice mismatch between graphene and Al_2O_3 (0001) is calculated to be ~10.8%. In addition, no obvious surface reconstruction of Al_2O_3 (0001) can be observed from the diffraction pattern (*13*). To further verify the structural information of the obtained graphene, we conducted TEM and selected area electron diffraction (SAED) measurements. Figure 3E displays a TEM image of the transferred graphene film on a TEM grid, verifying monolayer nature of our graphene. The intensity profile of the diffraction spots of SAED pattern (the solid yellow line in Fig. 3F) suggests the high quality of the monolayer graphene. Moreover, eight representative SAED patterns over a 10 μm by 10 μm area present similar crystallographic orientations, where the corresponding statistic of the angle distribution is less than 3.5°, in good agreement with the LEED results (Fig. 3, F and G, and fig. S10). The atomically resolved TEM

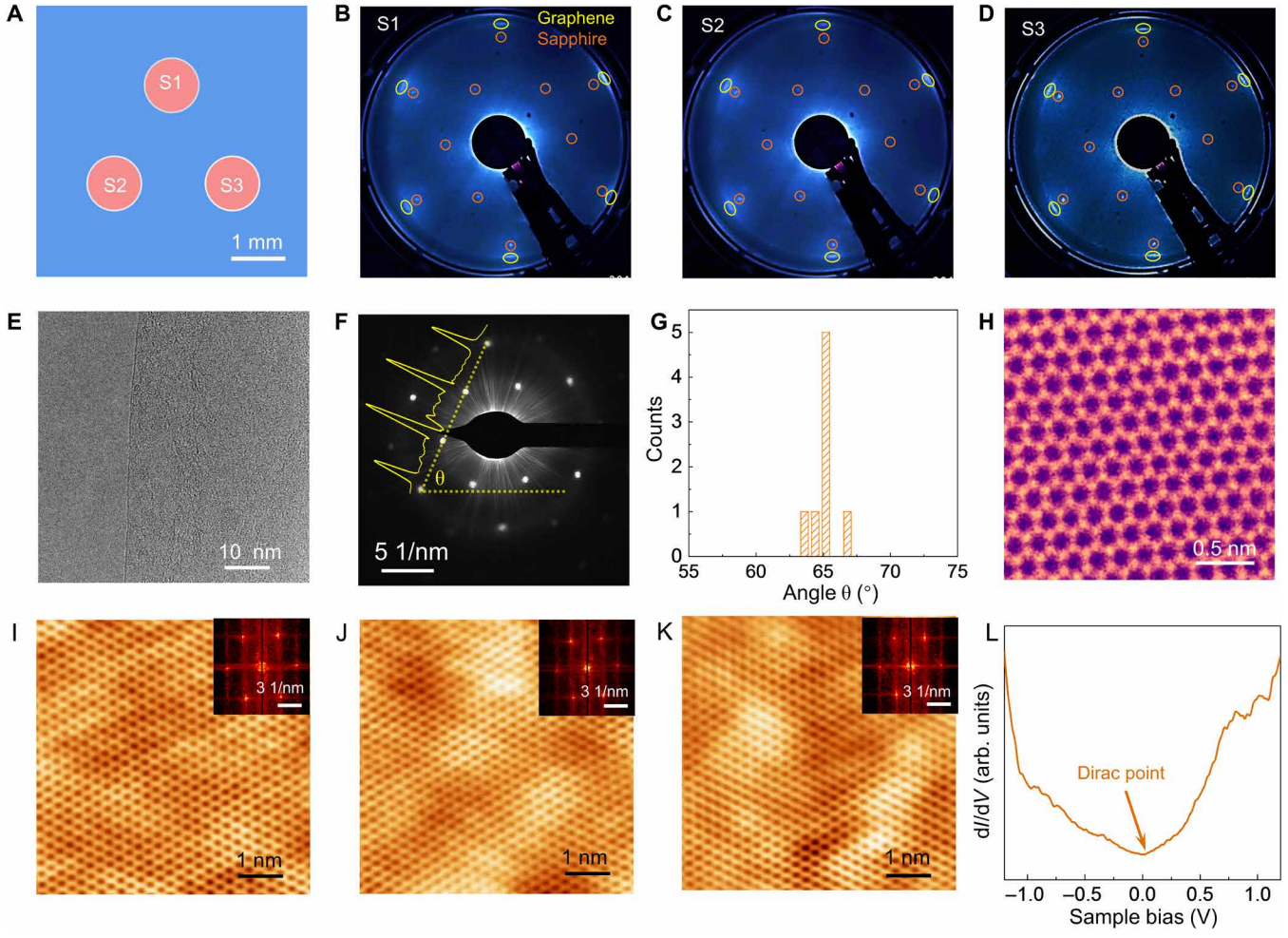

Fig. 3. High-quality graphene film consisting of highly oriented graphene domains. (**A**) Schematic diagram of the locations for LEED measurement on 5 mm by 5 mm graphene/sapphire. The diameter of the electron beam was ~1 mm. (**B** to **D**) Representative false color LEED patterns of as-grown graphene/sapphire at 70 eV. (**E**) TEM image on the edge of graphene film. (**F**) Typical SAED pattern of as-grown graphene. The inset shows the intensity profile of the diffraction pattern along the dashed yellow line, indicating the monolayer feature of the graphene. (**G**) Histogram of the angle distribution of SAED patterns randomly taken from 10 μm by 10 μm. (**H**) Atomically resolved scanning TEM image of as-grown graphene. (**I** to **K**) Three representative scanning tunneling microscopy (STM) images of as-grown graphene on sapphire in different areas along 2 μm with intervals of 1 μm. (**L**) Typical d*I*/d*V* spectrum of the as-grown graphene on sapphire.

image clearly shows the honeycomb lattice of graphene (Fig. 3H). In contrast, misorientation and small domain size occur at low growth temperatures in normal CVD system, e.g., 1100°C (fig. S11). The good alignment and large domain size of graphene benefit from the elevated growth temperature enabled by induction heating, which would promote nuclei to reach the most stable orientation.

We further used scanning tunneling microscopy (STM) to probe the stitching state of the graphene domains. Figure 3 (I to K) shows a set of STM images collected at different regions along a probing scale of 2 μm, all of which reveal a honeycomb lattice aligned unidirectionally without any defects, implying that the domain size is at least a few micrometers. Atomically resolved STM image further confirms that a continuous film can be obtained by the domain-domain stitching growth mode, with the presence of a small amount of grain boundary induced by merging those ill-aligned domains (fig. S12). STM observation further confirms the successful climbing over the sapphire steps, which is caused by carbon thermal reduction of sapphire (fig. S13) (*39*). In addition, the density of states is *V* shaped with the characteristic Dirac cone–like feature of single-layer graphene at ~0 eV in agreement with the observed honeycomb structure in topography (Fig. 3L). Collectively, we can conclude that thus grown graphene is a highly oriented film harnessing a high quality and purity.

Compared with the previously reported directly grown graphene, our highly oriented and large domain films should have improved electronic property. Macroscopic four-probe transport measurements were carried out to evaluate the large-scale electrical conductivity of the as-grown high-quality graphene on sapphire wafers. Figure 4A shows the sheet resistance map of a 2-inch graphene/sapphire wafer, where an average value as low as ca. (587 ± 40) ohms $\square^{-1}$ was observed. This result is markedly superior to those for graphene directly grown on glass substrates (*26*, *40*) and even comparative to those for graphene grown on polycrystalline Cu (*3*, *41*) and Ni foils (Fig. 4B) (*16*). The measured field-effect mobility of graphene on a sapphire substrate reached ~14,700 $cm^2 V^{-1} s^{-1}$ with a carrier density of 8×10^{11} cm^{-2} at 4 K (Fig. 4C) and 9500 $cm^2 V^{-1} s^{-1}$ with a carrier density of 9×10^{11} cm^{-2} at 300 K (fig. S14). A nondestructive terahertz time-domain spectroscopy approach was applied to map out the carrier mobility at a macroscopic scale with a fine resolution of 250 μm (*42*), accordingly manifesting a homogenous distribution of mobility values. As shown in Fig. 4D, more than 80% of the detected area affords a value higher than 6000 $cm^2 V^{-1} s^{-1}$ at room temperature. These values are markedly higher than previously reported ones for graphene directly grown on dielectric substrates (*18*, *26*, *40*), comparable to those from catalytic growth on metals (*3*, *41*, *43*) (table S1) and superior to those epitaxially grown on SiC in certain aspects (table S2). The low resistance and high mobility of obtained graphene films are mainly attributed to the remarkably reduced grain boundaries due to the enlarged domain size and good alignment, thereby holding promise in electronic and optoelectronic applications.

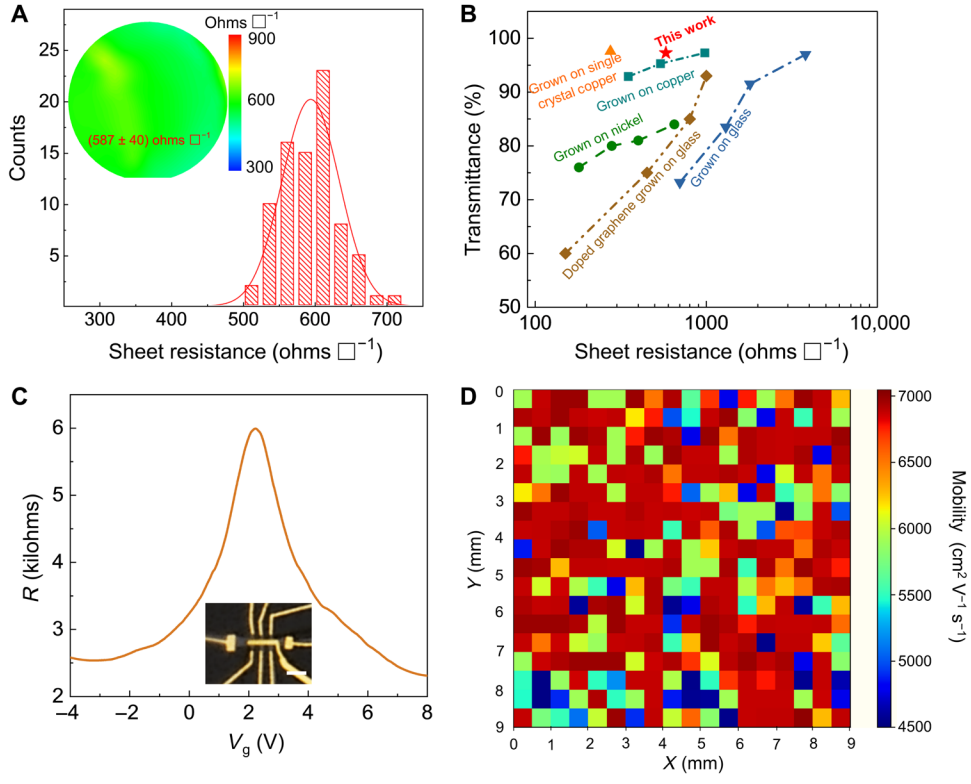

Fig. 4. Electrical properties of the as-grown highly oriented graphene. (**A**) Sheet resistance map of the 2-inch graphene/sapphire wafer. (**B**) Comparison of the sheet resistance versus optical transmission (at 550 nm) of directly gown graphene on sapphire in this work with previously reported pristine graphene and doped graphene grown on copper, nickel, and glass substrates. (**C**) Resistance of graphene versus the top gate voltage, and the nonlinear fitting of mobility is ~14,700 $cm^2 V^{-1} s^{-1}$ ($T = 4$ K). The inset shows OM image of the h-BN top-gated graphene Hall bar device. Scale bar, 2 μm (inset). (**D**) Terahertz large-size mobility mapping of the graphene film grown on sapphire at room temperature.

DISCUSSION

In conclusion, we have demonstrated the direct growth of wafer-scale, continuous, highly oriented, monolayer graphene film on *c*-plane (0001) sapphire with admirable quality via an electromagnetic induction heating CVD route. Such a synthetic solution allows quick temperature ramping up to 1400°C within 10 min and enables efficient pyrolysis of carbon feedstock/fast migration of active species. As confirmed by DFT calculations, the most stable graphene/Al_2O_3 configuration results in a well-aligned domain with a fixed orientation. Moreover, the reduced gas-phase temperature enables the homogeneous growth by suppressing the formation of multilayer nucleation and amorphous carbon. A high-quality continuous graphene wafer is accordingly obtained. Thus, the prepared graphene film shows a monolayer feature, high carrier mobility (14,700 $cm^2 V^{-1} s^{-1}$), and low sheet resistance (~587 ohms $\square^{-1}$). Encouragingly, the efficient and reliable synthesis of high-quality monolayer graphene directly on a sapphire wafer is compatible with back-end-of-line semiconductor processes, which would ultimately promote high-performance graphene electronics and industrialization.

MATERIALS AND METHODS

CVD growth of graphene on sapphire

Homemade electromagnetic induction heating cold wall CVD system was used for graphene growth. In detail, graphite wafer carrier located in the quartz chamber was shielded by insulation cladding and was heated by electromagnetic induction heating power. The growth temperature was monitored by pyrometers, and pressure can be tuned by closed-loop control. Typically, commercial 2-inch *c*-plane sapphire substrate (purchased from Unionlight Technology Co. Ltd) was directly placed on the graphite carrier and loaded into the chamber. The sapphire substrate was then heated to desired growth temperature (~1400°C) under a mixture of H_2 [500 standard cubic centimeters per minute (sccm)] and Ar (1000 sccm) at 2000 Pa and stabilized for ~5 min to avoid surface reconstruction (fig. S15). After that, graphene growth was performed by introducing CH_4 (100 sccm) as the carbon precursor for 10 to 30 min, while other parameters were kept constant. Upon CVD reaction, the sample was cooled down to room temperature under the protection of Ar and H_2 mixture.

Transport property measurements

h-BN was transferred onto the directly grown graphene/sapphire substrate and then directly fabricated into a Hall-bar device using a poly(methyl methacrylate) (PMMA) etching mask (PMMA 950K A4 at 4000 rpm) exposed by electron-beam lithography (FEI Nano-SEM 230) and Oxford deep reactive-ion etching. Afterward, 1-nm Cr and 50-nm Au were deposited on the samples using a thermal evaporator (Kurt J. Lesker Nano 36), followed by a standard metal liftoff technique. Electrical characterization was performed in an ICE Oxford 1K station using Keithley SourceMeter (Model 2000 and 2400).

Characterizations

The samples were characterized by OM (Olympus DX51), Raman spectroscopy (RAMAN WITEC ALPHA300R; 532-nm laser excitation, 100× objective lens), SEM (FEI Quattro S), four-probe system (CDE ResMap 178), AFM (Bruker Dimension Icon), x-ray photoelectron spectroscopy (Kratos Analytical Axis Ultra spectrometer using a monochromatic Al Kα x-ray source), terahertz time-domain spectroscopy (ONYX, das-Nano), TEM (FEI Tecnai F20; operating at 200 kV), aberration-corrected TEM (Nion U-HERMES 200; operated at 60 kV), and Omicron VT-STM/STS 330 system.

SUPPLEMENTARY MATERIALS

Supplementary material for this article is available at https://science.org/doi/10.1126/sciadv.abk0115

REFERENCES AND NOTES

1. K. S. Novoselov, V. I. Fal'ko, L. Colombo, P. R. Gellert, M. G. Schwab, K. Kim, A roadmap for graphene. *Nature* **490**, 192–200 (2012).
2. Y. Wu, Y.-m. Lin, A. A. Bol, K. A. Jenkins, F. Xia, D. B. Farmer, Y. Zhu, P. Avouris, High-frequency, scaled graphene transistors on diamond-like carbon. *Nature* **472**, 74–78 (2011).
3. S. Bae, H. Kim, Y. Lee, X. Xu, J.-S. Park, Y. Zheng, J. Balakrishnan, T. Lei, H. R. Kim, Y. I. Song, Y.-J. Kim, K. S. Kim, B. Ozyilmaz, J.-H. Ahn, B. H. Hong, S. Iijima, Roll-to-roll production of 30-inch graphene films for transparent electrodes. *Nat. Nanotechnol.* **5**, 574–578 (2010).
4. F. Xia, T. Mueller, Y.-m. Lin, A. Valdes-Garcia, P. Avouris, Ultrafast graphene photodetector. *Nat. Nanotechnol.* **4**, 839–843 (2009).
5. M. Liu, X. Yin, E. Ulin-Avila, B. Geng, T. Zentgraf, L. Ju, F. Wang, X. Zhang, A graphene-based broadband optical modulator. *Nature* **474**, 64–67 (2011).
6. T. Wu, X. Zhang, Q. Yuan, J. Xue, G. Lu, Z. Liu, H. Wang, H. Wang, F. Ding, Q. Yu, X. Xie, M. Jiang, Fast growth of inch-sized single-crystalline graphene from a controlled single nucleus on Cu-Ni alloys. *Nat. Mater.* **15**, 43–47 (2016).
7. J.-H. Lee, E. K. Lee, W.-J. Joo, Y. Jang, B.-S. Kim, J. Y. Lim, S.-H. Choi, S. J. Ahn, J. R. Ahn, M.-H. Park, C.-W. Yang, B. L. Choi, S.-W. Hwang, D. Whang, Wafer-scale growth of single-crystal monolayer graphene on reusable hydrogen-terminated germanium. *Science* **344**, 286–289 (2014).
8. J. L. Tedesco, B. L. VanMil, R. L. Myers-Ward, J. M. McCrate, S. A. Kitt, P. M. Campbell, G. G. Jernigan, J. C. Culbertson, C. R. Eddy Jr., D. K. Gaskill, Hall effect mobility of epitaxial graphene grown on silicon carbide. *Appl. Phys. Lett.* **95**, 122102 (2009).
9. E. Pallecchi, F. Lafont, V. Cavaliere, F. Schopfer, D. Mailly, W. Poirier, A. Ouerghi, High electron mobility in epitaxial graphene on 4H-SiC (0001) via post-growth annealing under hydrogen. *Sci. Rep.* **4**, 4558 (2014).
10. Y.-M. Lin, A. Valdes-Garcia, S.-J. Han, D. B. Farmer, I. Meric, Y. Sun, Y. Wu, C. Dimitrakopoulos, A. Grill, P. Avouris, K. A. Jenkins, Wafer-scale graphene integrated circuit. *Science* **332**, 1294–1297 (2011).
11. M. Kruskopf, D. M. Pakdehi, K. Pierz, S. Wundrack, R. Stosch, T. Dziomba, M. Götz, J. Baringhaus, J. Aprojanz, C. Tegenkamp, Comeback of epitaxial graphene for electronics: Large-area growth of bilayer-free graphene on SiC. *2D Mater.* **3**, 041002 (2016).
12. P. R. Whelan, V. Panchal, D. H. Petersen, D. M. Mackenzie, C. Melios, I. Pasternak, J. Gallop, F. W. Østerberg, P. U. Jepsen, W. Strupinski, O. Kazakova, P. Bøggild, Electrical homogeneity mapping of epitaxial graphene on silicon carbide. *ACS Appl. Mater. Interfaces* **10**, 31641–31647 (2018).
13. N. Mishra, S. Forti, F. Fabbri, L. Martini, C. McAleese, B. R. Conran, P. R. Whelan, A. Shivayogimath, B. S. Jessen, L. Buß, J. Falta, I. Aliaj, S. Roddaro, J. I. Flege, P. Bøggild, K. B. K. Teo, C. Coletti, Wafer-scale synthesis of graphene on sapphire: Toward fab-compatible graphene. *Small* **15**, 1904906 (2019).
14. X. Xu, Z. Zhang, L. Qiu, J. Zhuang, L. Zhang, H. Wang, C. Liao, H. Song, R. Qiao, P. Gao, Z. Hu, L. Liao, Z. Liao, D. Yu, E. Wang, F. Ding, H. Peng, K. Liu, Ultrafast growth of single-crystal graphene assisted by a continuous oxygen supply. *Nat. Nanotechnol.* **11**, 930–935 (2016).
15. Y. Hao, M. S. Bharathi, L. Wang, Y. Liu, H. Chen, S. Nie, X. Wang, H. Chou, C. Tan, B. Fallahazad, H. Ramanarayan, C. W. Magnuson, E. Tutuc, B. I. Yakobson, K. F. McCarty, Y.-W. Zhang, P. Kim, J. Hone, L. Colombo, R. S. Ruoff, The role of surface oxygen in the growth of large single-crystal graphene on copper. *Science* **342**, 720–723 (2013).
16. K. S. Kim, Y. Zhao, H. Jang, S. Y. Lee, J. M. Kim, K. S. Kim, J.-H. Ahn, P. Kim, J.-Y. Choi, B. H. Hong, Large-scale pattern growth of graphene films for stretchable transparent electrodes. *Nature* **457**, 706–710 (2009).
17. Z. Zhang, J. Du, D. Zhang, H. Sun, L. Yin, L. Ma, J. Chen, D. Ma, H.-M. Cheng, W. Ren, Rosin-enabled ultraclean and damage-free transfer of graphene for large-area flexible organic light-emitting diodes. *Nat. Commun.* **8**, 14560 (2017).
18. J. Chen, Y. Wen, Y. Guo, B. Wu, L. Huang, Y. Xue, D. Geng, D. Wang, G. Yu, Y. Liu, Oxygen-aided synthesis of polycrystalline graphene on silicon dioxide substrates. *J. Am. Chem. Soc.* **133**, 17548–17551 (2011).
19. W. Yang, G. Chen, Z. Shi, C.-C. Liu, L. Zhang, G. Xie, M. Cheng, D. Wang, R. Yang, D. Shi, K. Watanabe, T. Taniguchi, Y. Yao, Y. Zhang, G. Zhang, Epitaxial growth of single-domain graphene on hexagonal boron nitride. *Nat. Mater.* **12**, 792–797 (2013).
20. M. Kolmer, R. Zuzak, A.-K. Steiner, L. Zajac, M. Engelund, S. Godlewski, M. Szymonski, K. Amsharov, Fluorine-programmed nanozipping to tailored nanographenes on rutile TiO_2 surfaces. *Science* **363**, 57–60 (2019).

21. M. Kolmer, A.-K. Steiner, I. Izydorczyk, W. Ko, M. Engelund, M. Szymonski, A.-P. Li, K. Amsharov, Rational synthesis of atomically precise graphene nanoribbons directly on metal oxide surfaces. *Science* **369**, 571–575 (2020).
22. Z. Chen, Y. Qi, X. Chen, Y. Zhang, Z. Liu, Direct CVD growth of graphene on traditional glass: Methods and mechanisms. *Adv. Mater.* **31**, 1803639 (2019).
23. H. Kim, I. Song, C. Park, M. Son, M. Hong, Y. Kim, J. S. Kim, H.-J. Shin, J. Baik, H. C. Choi, Copper-vapor-assisted chemical vapor deposition for high-quality and metal-free single-layer graphene on amorphous SiO_2 substrate. *ACS Nano* **7**, 6575–6582 (2013).
24. P.-Y. Teng, C.-C. Lu, K. Akiyama-Hasegawa, Y.-C. Lin, C.-H. Yeh, K. Suenaga, P.-W. Chiu, Remote catalyzation for direct formation of graphene layers on oxides. *Nano Lett.* **12**, 1379–1384 (2012).
25. H. Wang, X. Xue, Q. Jiang, Y. Wang, D. Geng, L. Cai, L. Wang, Z. Xu, G. Yu, Primary nucleation-dominated chemical vapor deposition growth for uniform graphene monolayers on dielectric substrate. *J. Am. Chem. Soc.* **141**, 11004–11008 (2019).
26. L. Cui, X. Chen, B. Liu, K. Chen, Z. Chen, Y. Qi, H. Xie, F. Zhou, M. H. Rummeli, Y. Zhang, Z. Liu, Highly conductive nitrogen-doped graphene grown on glass toward electrochromic applications. *ACS Appl. Mater. Interfaces* **10**, 32622–32630 (2018).
27. T. Baehr-Jones, A. Spott, R. Ilic, A. Spott, B. Penkov, W. Asher, M. Hochberg, Silicon-on-sapphire integrated waveguides for the mid-infrared. *Opt. Express* **18**, 12127–12135 (2010).
28. Z. Chen, P. Gao, Z. Liu, Graphene-based LED: From principle to devices. *Acta Phys. -Chim. Sin.* **36**, 1907004 (2020).
29. J. Hwang, M. Kim, D. Campbell, H. A. Alsalman, J. Y. Kwak, S. Shivaraman, A. R. Woll, A. K. Singh, R. G. Hennig, S. Gorantla, M. H. Rüemmeli, M. G. Spencer, van der Waals epitaxial growth of graphene on sapphire by chemical vapor deposition without a metal catalyst. *ACS Nano* **7**, 385–395 (2013).
30. M. A. Fanton, J. A. Robinson, C. Puls, Y. Liu, M. J. Hollander, B. E. Weiland, M. LaBella, K. Trumbull, R. Kasarda, C. Howsare, J. Stitt, D. W. Snyder, Characterization of graphene films and transistors grown on sapphire by metal-free chemical vapor deposition. *ACS Nano* **5**, 8062–8069 (2011).
31. Z. Chen, H. Chang, T. Cheng, T. Wei, R. Wang, S. Yang, Z. Dou, B. Liu, S. Zhang, Y. Xie, Z. Liu, Y. Zhang, J. Li, F. Ding, P. Gao, Z. Liu, Direct growth of nanopatterned graphene on sapphire and its application in light emitting diodes. *Adv. Funct. Mater.* **30**, 2001483 (2020).
32. H. J. Song, M. Son, C. Park, H. Lim, M. P. Levendorf, A. W. Tsen, J. Park, H. C. Choi, Large scale metal-free synthesis of graphene on sapphire and transfer-free device fabrication. *Nanoscale* **4**, 3050–3054 (2012).
33. K. Jia, H. Ci, J. Zhang, Z. Sun, Z. Ma, Y. Zhu, S. Liu, J. Liu, L. Sun, X. Liu, J. Sun, W. Yin, H. Peng, L. Lin, Z. Liu, Superclean growth of graphene using a cold-wall chemical vapor deposition approach. *Angew. Chem. Int. Ed.* **59**, 17214–17218 (2020).
34. X. G. Wang, A. Chaka, M. Scheffler, Effect of the environment on alpha-Al_2O_3 (0001) surface structures. *Phys. Rev. Lett.* **84**, 3650–3653 (2000).
35. Z. Dou, Z. Chen, N. Li, S. Yang, Z. Yu, Y. Sun, Y. Li, B. Liu, Q. Luo, T. Ma, L. Liao, Z. Liu, P. Gao, Atomic mechanism of strong interactions at the graphene/sapphire interface. *Nat. Commun.* **10**, 5013 (2019).
36. J. Sun, Y. Chen, M. K. Priydarshi, Z. Chen, A. Bachmatiuk, Z. Zou, Z. Chen, X. Song, Y. Gao, M. H. Ruemmeli, Y. Zhang, Z. Liu, Direct chemical vapor deposition-derived graphene glasses targeting wide ranged applications. *Nano Lett.* **15**, 5846–5854 (2015).
37. H. Huang, W. Chen, S. Chen, A. T. S. Wee, Bottom-up growth of epitaxial graphene on 6H-SiC (0001). *ACS Nano* **2**, 2513–2518 (2008).
38. K. V. Emtsev, A. Bostwick, K. Horn, J. Jobst, G. L. Kellogg, L. Ley, J. L. McChesney, T. Ohta, S. A. Reshanov, J. Röhrl, E. Rotenberg, A. K. Schmid, D. Waldmann, H. B. Weber, T. Seyller, Towards wafer-size graphene layers by atmospheric pressure graphitization of silicon carbide. *Nat. Mater.* **8**, 203–207 (2009).
39. J. H. Cox, L. Pidgeon, An investigation of the aluminum–oxygen–carbon system. *Can. J. Chem.* **41**, 671–683 (1963).
40. X.-D. Chen, Z. Chen, W.-S. Jiang, C. Zhang, J. Sun, H. Wang, W. Xin, L. Lin, M. K. Priydarshi, H. Yang, Z.-B. Liu, J.-G. Tian, Y. Zhang, Y. Zhang, Z. Liu, Fast growth and broad applications of 25-inch uniform graphene glass. *Adv. Mater.* **29**, 1603428 (2017).
41. J. W. Suk, A. Kitt, C. W. Magnuson, Y. Hao, S. Ahmed, J. An, A. K. Swan, B. B. Goldberg, R. S. Ruoff, Transfer of CVD-grown monolayer graphene onto arbitrary substrates. *ACS Nano* **5**, 6916–6924 (2011).
42. P. Bøggild, D. M. Mackenzie, P. R. Whelan, D. H. Petersen, J. D. Buron, A. Zurutuza, J. Gallop, L. Hao, P. U. Jepsen, Mapping the electrical properties of large-area graphene. *2D Mater.* **4**, 042003 (2017).
43. C. Liu, X. Xu, L. Qiu, M. Wu, R. Qiao, L. Wang, J. Wang, J. Niu, J. Liang, X. Zhou, Z. Zhang, M. Peng, P. Gao, W. Wang, X. Bai, D. Ma, Y. Jiang, X. Wu, D. Yu, E. Wang, J. Xiong, F. Ding, K. Liu, Kinetic modulation of graphene growth by fluorine through spatially confined decomposition of metal fluorides. *Nat. Chem.* **11**, 730–736 (2019).
44. G. Kresse, J. Hafner, Ab initio molecular dynamics for liquid metals. *Phys. Rev. B* **47**, 558–561 (1993).
45. P. E. Blöchl, Projector augmented-wave method. *Phys. Rev. B* **50**, 17953–17979 (1994).
46. J. P. Perdew, K. Burke, M. Ernzerhof, Generalized gradient approximation made simple. *Phys. Rev. Lett.* **77**, 3865–3868 (1996).
47. H. J. Monkhorst, J. D. Pack, Special points for Brillouin-zone integrations. *Phys. Rev. B* **13**, 5188–5192 (1976).
48. J. Klimeš, D. R. Bowler, A. Michaelides, Van der Waals density functionals applied to solids. *Phys. Rev. B* **83**, 195131 (2011).
49. P. T. M. M. van Attekum, G. K. Wertheim, Excitonic effects in core-hole screening. *Phys. Rev. Lett.* **43**, 1896–1898 (1979).
50. S. Doniach, M. Sunjic, Many-electron singularity in x-ray photoemission and x-ray line spectra from metals. *J. Phys. C Solid State Phys.* **3**, 285–291 (1970).
51. S. Tang, H. Wang, H. S. Wang, Q. Sun, X. Zhang, C. Cong, H. Xie, X. Liu, X. Zhou, F. Huang, X. Chen, T. Yu, F. Ding, X. Xie, M. Jiang, Silane-catalysed fast growth of large single-crystalline graphene on hexagonal boron nitride. *Nat. Commun.* **6**, 6499 (2015).
52. W. S. Leong, H. Wang, J. Yeo, F. J. Martin-Martinez, A. Zubair, P.-C. Shen, Y. Mao, T. Palacios, M. J. Buehler, J.-Y. Hong, J. Kong, Paraffin-enabled graphene transfer. *Nat. Commun.* **10**, 867 (2019).
53. B. Deng, Z. Pang, S. Chen, X. Li, C. Meng, J. Li, M. Liu, J. Wu, Y. Qi, W. Dang, H. Yang, Y. Zhang, J. Zhang, N. Kang, H. Xu, Q. Fu, X. Qiu, P. Gao, Y. Wei, Z. Liu, H. Peng, Wrinkle-free single-crystal graphene wafer grown on strain-engineered substrates. *ACS Nano* **11**, 12337–12345 (2017).
54. J. Robinson, X. Weng, K. Trumbull, R. Cavalero, M. Wetherington, E. Frantz, M. LaBella, Z. Hughes, M. Fanton, D. Snyder, Nucleation of epitaxial graphene on SiC (0001). *ACS Nano* **4**, 153–158 (2010).
55. J. Kim, H. Park, J. B. Hannon, S. W. Bedell, K. Fogel, D. K. Sadana, C. Dimitrakopoulos, Layer-resolved graphene transfer via engineered strain layers. *Science* **342**, 833–836 (2013).

Acknowledgments: We thank K. Wu, B. Feng from Institute of Physics, Chinese Academy of Sciences, and J. Hu from National University of Singapore for discussions and V. De Miguel from das-Nano and Z. Gong from Quantum Design China (Beijing) Co. Ltd. for terahertz mobility measurement. We acknowledge Electron Microscopy Laboratory in Peking University for the use of Cs-corrected electron microscope. The DFT calculations were carried out on TianHe-1(A) at the National Supercomputer Center in Tianjin. **Funding:** This work was financially supported by the National Key R&D Program of China (2019YFA0708201 and 2019YFA0708204), National Natural Science Foundation of China (51520105003, 51861135201, 51672007, 51702225, 11974023, and 12074369), Beijing Municipal Natural Science Foundation (Z191100000819004), Suzhou Science and Technology Project-Prospective Application Research Program (SYG202038), Key R&D Program of Guangdong Province (2018B030327001 and 2018B010109009), National Equipment Program of China (ZDYZ2015-1), and "2011 Program" Peking-Tsinghua-IOP Collaborative Innovation Center for Quantum Matter. K.S.N. acknowledges support from the Ministry of Education (Singapore) through the Research Centre of Excellence program (Award EDUN C-33-18-279-V12, Institute for Functional Intelligent Materials). **Author contributions:** Z.C., P.G., Jingyu S., and Z.L. conceived and designed the experiments. Z.C. performed the experiments. S.Y. did the theoretical calculations. B.L., P.G., performed the TEM characterizations. C.X., M.H., and Y.Z. did the STM characterization. X.W., L.H., and X.L. conducted the LEED measurement. Z.C., J.Z., W.W., and L.L. fabricated and measured the Hall bar device under the guidance of K.S.N. Jingyuan S.and X.G. are responsible for technical assistance with graphene growth. Z.C. performed the data analysis and wrote the manuscript under the direction of S.Y., P.G., Y.Z., K.S.N., Jingyu S., and Z.L. All authors contributed to the discussion and analysis of the results. **Competing interests:** The authors declare that they have no competing financial interests. **Data and materials availability:** All data needed to evaluate the conclusions in the paper are present in the paper and/or the Supplementary Materials.

Submitted 16 June 2021
Accepted 1 October 2021
Published 19 November 2021
10.1126/sciadv.abk0115